Reconfigurable Channel Slicing and Stitching for an Optical Signal to Enable Fragmented Bandwidth Allocation Using Nonlinear Wave Mixing and an Optical Frequency Comb

Yinwen Cao, Ahmed Almaiman, Morteza Ziyadi, Amirhossein Mohajerin-Ariaei, Changjing Bao, Peicheng Liao, Fatemeh Alishahi, Ahmad Fallahpour, Youichi Akasaka, Carsten Langrock, Martin M. Fejer, *Fellow, IEEE*, Joseph D. Touch, *Senior Member, IEEE*, Moshe Tur, *Fellow, IEEE*, and Alan E. Willner, *Fellow, IEEE*

(Top-Scored Paper)

***Abstract*—A scheme for reconfigurable channel slicing and stitching is proposed and experimentally demonstrated. By employing optical nonlinear wave mixing and a coherent frequency comb, a single channel spectrum is sliced and redistributed into fragmented frequency slots, which can be stitched together to recover the original channel at the receiver. This approach is verified through a single channel experiment with the modulation formats of quadrature phase-shift keying and 16 quadrature amplitude modulation. The system exhibits less than 1.5% error-vector-magnitude deterioration and no more than 2-dB optical signal-to-noise ratio penalty, compared to a back-to-back baseline. To demonstrate robustness of the scheme, different parameters of the channel slices are varied, such as relative phase offset, relative amplitude, and the number of slices. A 10-km transmission experiment is also conducted and the additional system penalty is negligible. This scheme is used to experimentally demonstrate fragmented channel bandwidth allocation in a dense 6-channel wavelength-division-multiplexing system. The incoming 20-Gbaud optical channel is successfully reallocated into two fragmented frequency slots and reconstructed at thereceiver.**

***Index Terms*—Inter-channel interference, optical frequency comb, optical wavelength conversion, WDM networks.**

Manuscript received June 25, 2017; revised August 18, 2017; accepted September 3, 2017. Date of publication September 7, 2017; date of current version February 24, 2018. This work was supported in part by the National Science Foundation (NSF) Center for Integrated Access Networks under Grant Y501119, in part by the NSF Optical Tapped-Delay-Line under Grant ECCS-1202575, in part by the Fujitsu Laboratories of America, and in part by the National Institute of Standards and Technology under Grant 70NANB16H012. *(Corresponding author: Yinwen Cao.)*

Y. Cao, A. Almaiman, M. Ziyadi, A. Mohajerin-Ariaei, C. Bao, P. Liao, F. Alishahi, A. Fallahpour, and A. E. Willner are with the Ming Hsieh Department of Electrical Engineering, University of Southern California, Los Angeles, CA 90089 USA (e-mail: yinwenca@usc.edu; almaiman@usc.edu; ziyadi@usc.edu; mohajera@usc.edu; changjib@usc.edu; peicheng@usc.edu; falishah@usc.edu; fallahpo@usc.edu; willner@usc.edu).

Y. Akasaka is with the Fujitsu Laboratories of America, Richardson, TX 75082 USA (e-mail: youichi.akasaka@us.fujitsu.com).

C. Langrock and M. M. Fejer are with the Edward L. Ginzton Laboratory, Stanford University, Stanford, CA 94305 USA (e-mail: langrock@stanford.edu; fejer@stanford.edu).

J. D. Touch is with the Information Sciences Institute, University of Southern California, Marina del Rey, CA 90292 USA (e-mail: touch@isi.edu).

M. Tur is with the School of Electrical Engineering, Tel Aviv University, Tel Aviv 69978, Israel (e-mail: tur@post.tau.ac.il).

Color versions of one or more of the figures in this paper are available online at http://ieeexplore.ieee.org.

Digital Object Identifier 10.1109/JLT.2017.2750168

I. Introduction

ELASTIC optical networks (EONs) are becoming of great interest owing to their ability to handle heterogeneous data channels with flexible bandwidths [1]–[6]. Fragmented bandwidth allocation would be crucial in EONs to ensure the efficient use of the precious optical transmission spectrum. A key function of fragmented bandwidth allocation is the capability of adding a given data channel into any available fragmented frequency slots [7]. As an example, consider a situation in which an optical channel with a 200 GHz bandwidth is requested while the current optical network can provide only two separate spectral regions of 50 GHz and 150 GHz. A straightforward approach would be to (i) down-convert the 200 GHz optical data channel to the electrical/digital domain; (ii) decompose the original channel into two sub-channels with bandwidths of 50 GHz and 150 GHz separately; (iii) generate two optical channels that “fit” within the two available spectral regions by using two optical transmitters; (iv) reverse the sequence on reception to restore the 200 GHz channel.

However, it might be valuable to achieve this goal using high-speed optical signal processing, in order to avoid inefficient optical-electrical-optical (O-E-O) conversion. In this case, the original data channel is optically sliced into several partial frequency components, which could be assigned into the available fragmented frequency slots with the assistance of optical wavelength conversion. On reception, the sliced components are stitched together for channel reconstruction.

This paper proposes the use of nonlinear wave mixing and a coherent optical frequency comb to implement reconfigurable channel slicing and stitching for an optical signal [8]. Feasibility of this approach is experimentally demonstrated using quadrature phase-shift keying (QPSK) and 16 quadrature amplitude modulation (16QAM). The system performance is evaluated

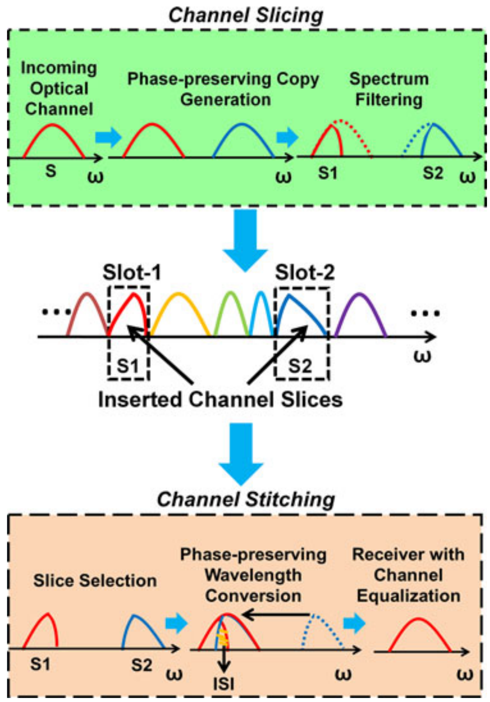

Fig. 1. Conceptual diagram of fragmented bandwidth allocation enabled by channel slicing and stitching.

by tuning different parameters. In addition to investigating the effect of relative phase offset as described in [8], we further explore: (i) the influence of the relative amplitude and the number of channel slices on system performance; (ii) a 10-km transmission experiment compared to a back-to-back (B2B) scenario. One application of the channel slicing and stitching is to enable fragmented bandwidth allocation, which is experimentally demonstrated in a dense 6-channel wavelength-division-multiplexing (WDM) system. The experimental results show that the incoming 20 Gbaud optical QPSK channel is successfully reallocated into two available fragmented frequency slots and reconstructed at the receiver by using channel slicing and stitching.

II. Concept

The conceptual diagram of fragmented bandwidth allocation enabled by channel slicing and stitching is illustrated in Fig. 1. Assume the current optical spectrum is occupied by multiple data channels with only two small frequency slots (Slot-1 and Slot-2) available. The incoming optical channel (S) has a large bandwidth that cannot be accommodated by any single frequency slot without introducing severe inter-channel interference (ICI) from spectrum overlapping. However, the total bandwidth of the separate available frequency slots is larger than that of channel S. In this case, channel S can be sliced into two spectral fragments, which are then reallocated into the available frequency slots. The detail of this process is shown in Fig. 1. In the beginning, a coherent copy of channel S is generated at another wavelength by nonlinear wave mixing of channel S with an optical frequency comb [9], [10]. After channel copy generation, an optical filter is employed to slice partial spectra of the two channels. It is noted that the combination of the two output channel slices (S1 and S2) should preserve all the information of the original channel S. Then, S1 and S2 are narrow enough to be inserted into the two frequency slots for transmission.

To reconstruct the original channel S at the receiver, the two channel slices S1 and S2 are first selected from the current WDM system. Then, another stage of comb-based wavelength conversion is employed to recombine S1 and S2 in phase for channel recovery. Because of nonideal filtering in both stages of spectrum filtering and slice selection, S1 and S2 may have a partially overlapped spectrum, which can then produce inter-symbol interference (ISI), as shown in Fig. 1. However, the effect of ISI can be readily compensated by a digital linear equalizer afterwards and the original channel S can ultimately be recovered. Note that this channel slicing and stitching technique is scalable to more than two slices simply by generating more copies of the original data channel and by following the procedure shown in Fig. 1.

III. Experimental Setup for Feasibility Demonstration in a Single Channel System

The previous section indicates that the key function to achieving fragmented bandwidth allocation is the channel slicing and stitching. Fig. 2 shows a single channel experimental setup to demonstrate this function.

At the transmitter, the data signal with the format of 20/28 Gbaud QPSK (and alternatively 20 Gbaud 16QAM) modulates a laser at the wavelength of 1542.53 nm in an optical IQ modulator. Note that the output optical signal is not pulse shaped. At the same time, an optical frequency comb with a 20 GHz repetition rate is generated by a mode-locked laser (MLL). In the case of slicing channel spectrum into two parts (S1 and S2), two comb lines at the wavelengths of 1538.90 nm and 1539.86 nm are selected by a spatial light modulator (SLM-1) filter. The wavelength difference between the two comb lines determines the wavelength shift of the channel copy, which is generated in the next step.

In the following, both the signal (S) and the selected comb lines are amplified and injected into a periodically poled lithium niobate (PPLN-1) waveguide with a quasi-phase matching (QPM) wavelength of 1541.00 nm. After PPLN-1, a channel copy is generated, albeit with 10 dB lower power due to the conversion efficiency. The input and output of PPLN-1 are shown in Fig. 3(a) and (b). Then, another SLM filter (SLM-2) is used to cut a left slice (S1) from the original channel and a right slice (S2) from the channel copy. The corresponding spectrum is shown in Fig. 3(c), in which the optical channel bandwidths of S1 and S2 are ∼27 GHz and ∼18 GHz, respectively. Afterwards, S1 and S2 are sent to either (i) channel stitching for the signal reconstruction, or (ii) a 10-km single mode fiber (SMF) for transmission.

Before the receiver, S1 and S2 are amplified and mixed with two comb lines with the same wavelength difference in a second PPLN (PPLN-2) of the same QPM wavelength, as shown in Fig. 3(d). After PPLN-2, S1 is shifted to the right with a

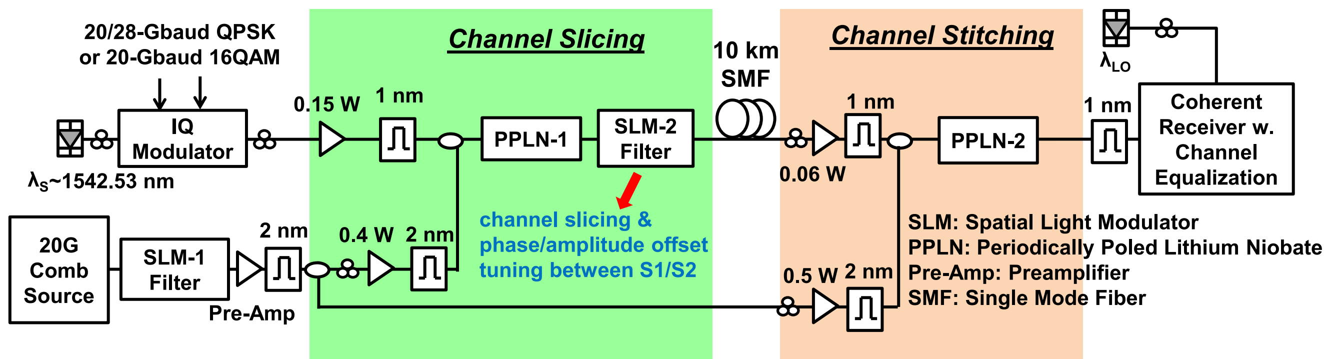

Fig. 2. Experimental setup of channel slicing and stitching for a single optical channel. The optical frequency comb is employed to achieve phase-preserving channel copy generation and channel slices recombination (stitching).

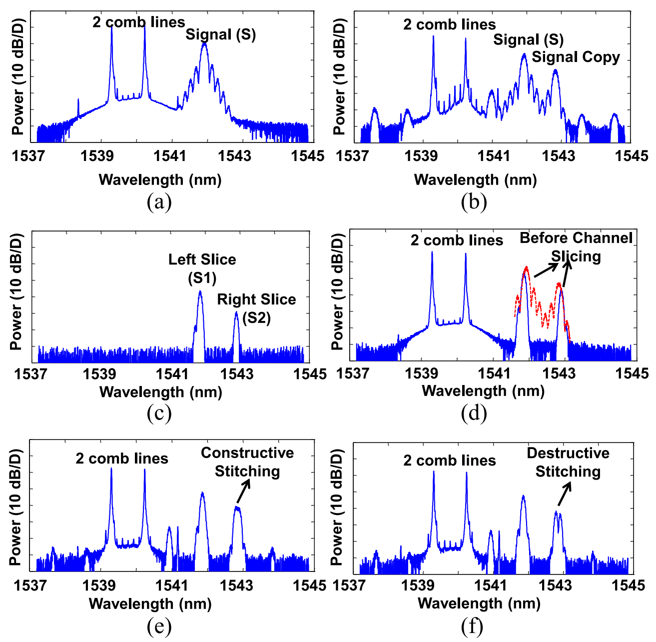

Fig. 3. Measured spectra: (a) before PPLN-1; (b) after PPLN-1; (c) after SLM-2 filter; (d) before PPLN-2; (e) after PPLN-2 with constructive channel stitching; (f) after PPLN-2 with destructive channel stitching.

conversion efficiency of -10 dB and recombined with S2. Since S2 is about 10 dB lower than S1 as shown in Fig. 3(c), the two channel slices will now be combined with almost the same power. Because of nonideal filtering, S1 and S2 have $\sim$5 GHz partial spectrum overlap. As a result of this overlap, tuning the phase offset ($\Delta\varphi$) between S1 and S2 in SLM-2 can lead to constructive ($\Delta\varphi = 0$) or destructive ($\Delta\varphi = 180°$) channel stitching. As shown in Fig. 3(e) and (f), destructive stitching should be avoided due to the loss of partial channel spectrum. Finally, the stitched channel is filtered out and sent to an optical coherent receiver. Based on a conventional decision-directed algorithm [11], digital channel equalization with 11 taps is used to remove spectrum-overlapping-induced ISI. If the amount of spectrum overlap increases, more taps might be required to compensate for the increased ISI.

Note that in Fig. 3(a), the input optical signal includes both the fundamental band and side lobes. The peak power difference

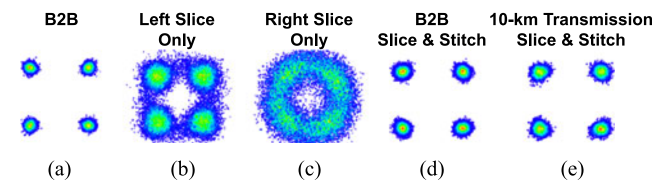

Fig. 4. Constellation comparison of a 20 Gbaud QPSK channel under different scenarios: (a) B2B without channel slicing and stitching; (b) detection of only the left channel slice; (c) detection of only the right channel slice; (d) B2B with channel slicing and stitching; (e) after 10-km transmission with channel slicing and stitching.

between them is more than 15 dB, and we do not observe a significant contribution of the side lobes to the signal quality. Therefore, the output signal is allowed to primarily be composed of the fundamental band component, and we consider the channel bandwidth to be the frequency range of the fundamental band component. Moreover, in order to use channel slicing and stitching for the given WDM grid: (i) the bandwidth of the input signal should be larger than the spectral grid spacing; and (ii) the bandwidths of the sliced signals should be smaller than the spectral grid spacing.

IV. Experimental Results for a Single Channel System

Fig. 4 shows constellation diagrams of a 20 Gbaud QPSK channel with 30 dB OSNR under different scenarios. Compared to a B2B baseline shown in Fig. 4(a), Fig. 4(b) and (c) indicates that the channel quality deteriorates if only a partial spectrum is detected. The different constellations between the left and right slices are the result of unequal bandwidths of the two slices. Fig. 4(d) shows that the channel is successfully recovered after channel stitching of the left and right slices. The signal quality is almost preserved after 10-km transmission as shown in Fig. 4(e), because the channel equalization at the receiver also compensates for chromatic dispersion [12]–[14].

The system performance is further evaluated by tuning the relative phase offset ($\Delta\varphi$) and relative amplitude ($\Delta\alpha$) between S1 and S2 in SLM-2. The reason to investigate the impact of phase/amplitude imbalance is because the two parameters could affect the performance of channel stitching. In Fig. 5, when the phase is aligned ($\Delta\varphi = 0$), channel equalization can compensate for the ISI effect due to the partial spectrum overlapping of

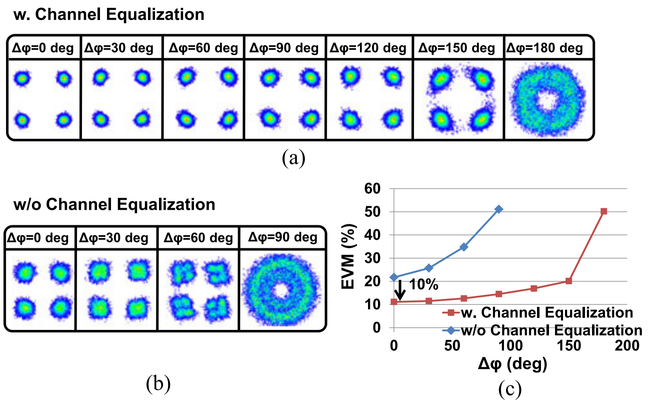

Fig. 5. Constellation comparison of a 20 Gbaud QPSK by tuning the relative phase offset ($\Delta\varphi$) between two channel slices: (a) with channel equalization; (b) without channel equalization. (c) Measured EVMs with different $\Delta\varphi$.

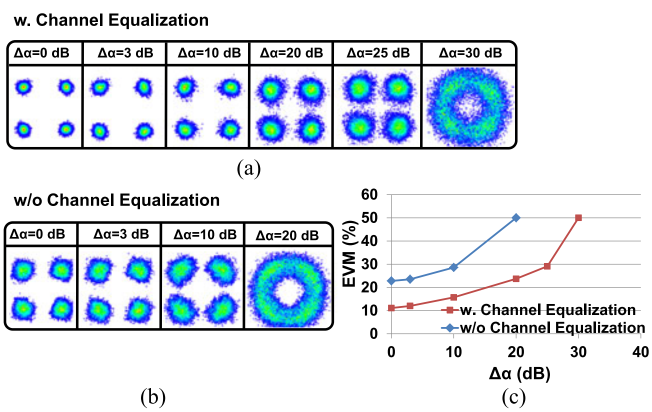

Fig. 6. Constellation comparison of a 20 Gbaud QPSK by tuning the relative amplitude ($\Delta\alpha$) between two channel slices: (a) with channel equalization; (b) without channel equalization. (c) Measured EVMs with different $\Delta\alpha$.

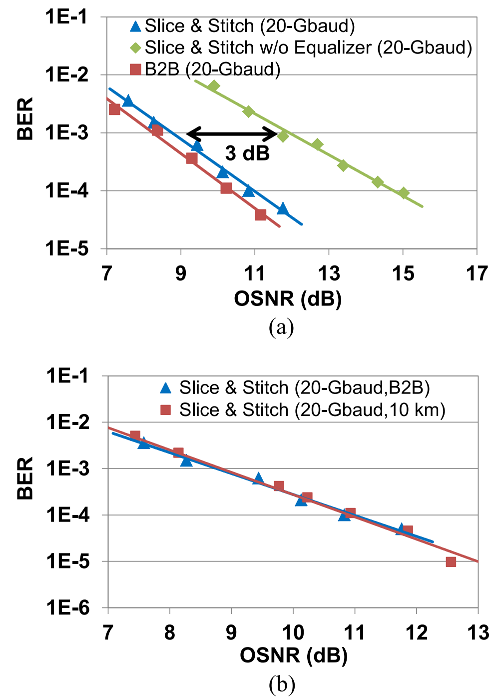

Fig. 7. BER comparison for a 20 Gbaud QPSK system: (a) with and without digital equalization; (b) B2B and 10-km transmission.

the left and right channel slices. Channel equalization helps to decrease the error-vector-magnitude (EVM) from $\sim$20% down to $\sim$10%, as shown in Fig. 5(c). Additionally, the tolerance of $\Delta\varphi$ can be as large as 150° with channel equalization, whereas the system without channel equalization fails if $\Delta\varphi$ is 90°. Similarly, in terms of the relative amplitude $\Delta\alpha$, the system with channel equalization can still work when $\Delta\alpha$ is 25 dB, whereas an equalization-free system cannot tolerate $\Delta\alpha$ of 20 dB.

As a result, digital channel equalization not only enhances the performance of channel stitching by compensating for ISI, but it also increases the system tolerance for phase/amplitude imbalance. Additionally, a lower signal EVM can be obtained if the phase/amplitude imbalance is pre-compensated optically by SLM-2, as shown in Figs. 5(a), (c) and 6(a), (c). Therefore, in the remainder of the paper: (i) channel equalization is included primarily to compensate for ISI; and (ii) the phase/amplitude imbalance is pre-compensated in the optical domain.

Fig. 7 shows the measured BER curves of the system. Compared to a B2B baseline system, the optical signal-to-noise ratio (OSNR) penalty of channel slicing and stitching with channel equalization is below 1 dB, as shown in Fig. 7(a). It is noted that for the B2B baseline system, the same channel equalization is used for comparison. In addition, the two nearly overlapping BER curves in Fig. 7(b) indicate the system penalty for the 10-km transmission is negligible. For longer-distance transmission, the increased chromatic dispersion, as well as the wavelength-dependent polarization rotation caused by higher order polarization mode dispersion (PMD), could affect the phase alignment among different channel slices. As a result, the performance of channel stitching might be degraded, which requires further investigation.

The spectra of the channel slicing and stitching with 3 channel slices of a 28 Gbaud QPSK channel are shown in Fig. 8(a)–(c), while the corresponding separate channel slices and reconstructed channel constellations are shown in Fig. 8(d).

The BER curves of the 28 Gbaud QPSK system with two and three channel slices are presented in Fig. 9. It can be seen that the system performance does not strongly depend on the number of channel slices, and less than 1 dB OSNR penalty is observed compared to the B2B baseline.

The scheme is extended to a 20 Gbaud 16QAM signal. Less than 1.5% EVM deterioration with 30 dB OSNR is observed, as shown in Fig. 10(a). Compared to the QPSK scenario in Fig. 7(a), a larger OSNR penalty is observed for 16QAM in Fig. 10(b). A possible reason could be that high order QAM signals are more sensitive to any distortion introduced by nonlinear-wave-mixing-based wavelength conversion [15].

V. Experimental Setup for Fragmented Bandwidth Allocation in a WDM System

The application of channel slicing and stitching to enable fragmented bandwidth allocation is experimentally demonstrated

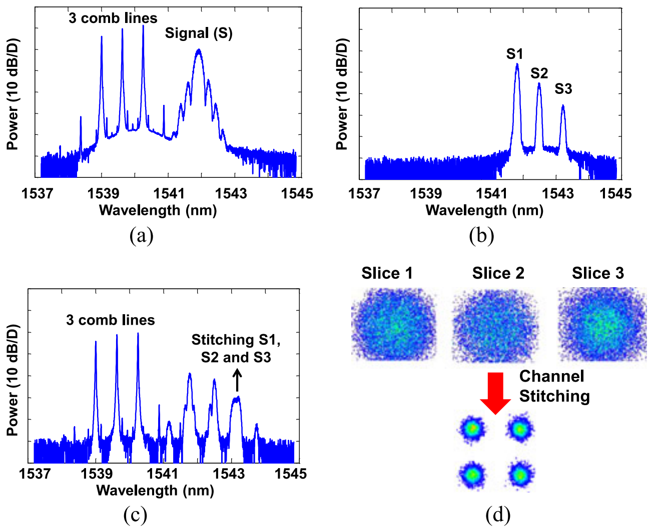

Fig. 8. Channel slicing and stitching with three slices for a 28 Gbaud QPSK system: (a) optical spectrum before PPLN-1; (b) optical spectrum after SLM-2 filter; (c) optical spectrum after PPLN-2; (d) channel reconstruction by stitching three channel slices.

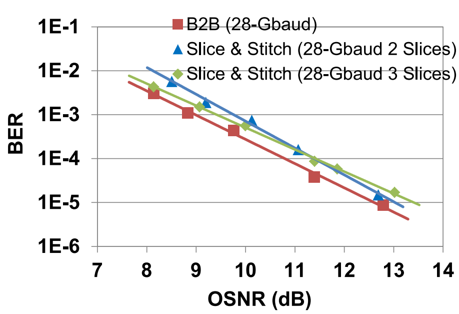

Fig. 9. BER comparison with different numbers of channel slices.

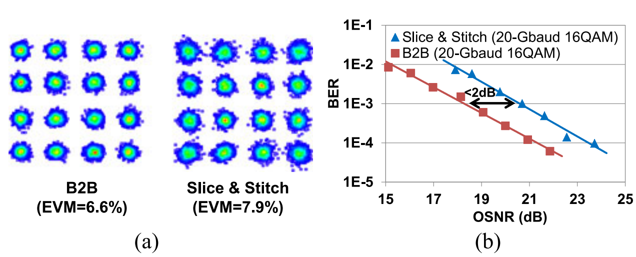

Fig. 10. (a) EVM comparison between B2B and channel slicing and stitching for a 20 Gbaud 16QAM signal; (b) BER comparison.

in a WDM system with 6 QPSK channels of 20 Gbaud. The experimental setup is shown in Fig. 11(a) and the central wavelengths of the 6 channels are 1541.68, 1542.00, 1542.16, 1542.32, 1542.52, and 1542.87 nm. Compared to the single-channel experiment shown in Fig. 2, a stage of WDM channel generation is added, as shown by the dotted box. In this case, the attenuator is used to adjust the power of the WDM channels, in order to make it similar to that of the added optical channel S. After the attenuator, a polarization controller is used to align the polarization of the WDM channels with that of

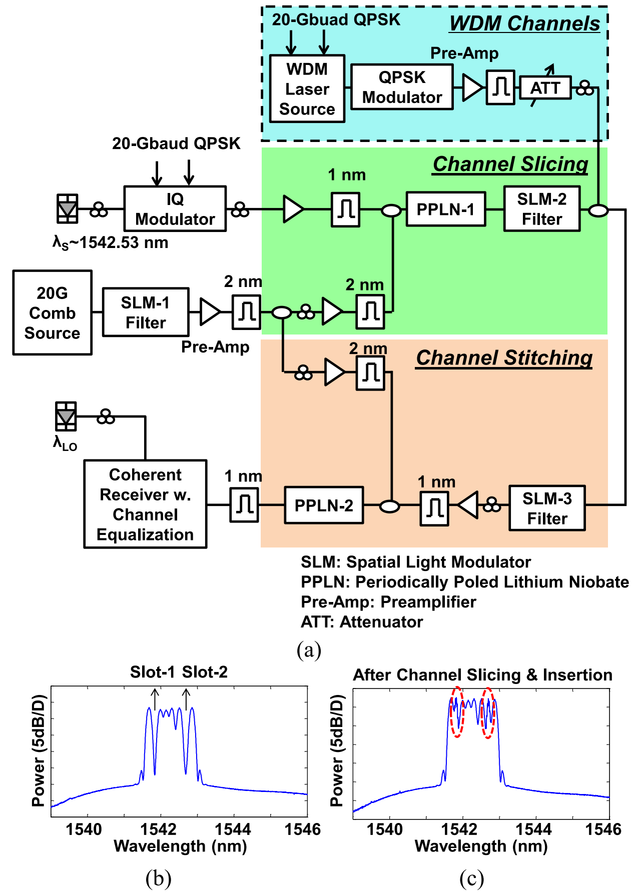

Fig. 11. (a) Experimental setup for fragmented bandwidth allocation in 20 Gbaud QPSK WDM channels; (b) measured spectrum before fragmented bandwidth allocation; (c) measured spectrum after fragmented bandwidth allocation.

channel S in order to maximize the ICI effect. The optical spectra before and after fragmented bandwidth allocation are shown in Fig. 11(b) and (c), in which the two sliced channels each have ~22 GHz optical bandwidth. At the receiver, an extra SLM filter (SLM-3) is used for channel-slice selection and amplitude/phase adjustment. In order to allocate the same power into the two frequency slots, the channel slice with higher power is attenuated by 10 dB in SLM-2 to offset the effect of the −10 dB conversion efficiency in PPLN-1. Subsequently, the power difference is adjusted in SLM-3 before channel stitching in PPLN-2.

VI. Experimental Results for a WDM System

The constellation comparison is shown in Fig. 12. Compared to direct channel insertion shown in Fig. 12(c) and (d), where the entire channel S is inserted into either Slot-1 or Slot-2, fragmented bandwidth allocation can effectively avoid channel spectrum overlapping and therefore suffer much less ICI penalty. The reason for signal quality deterioration in Fig. 12(b) compared to the single-channel scenario in Fig. 12(a) might be attributed to nonideal filtering for selecting channel slices, which includes the residual spectra from adjacent channels.

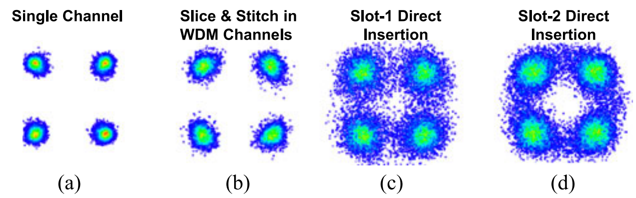

Fig. 12. Constellation comparison between direct channel insertion and fragmented bandwidth allocation enabled by channel slicing and stitching.

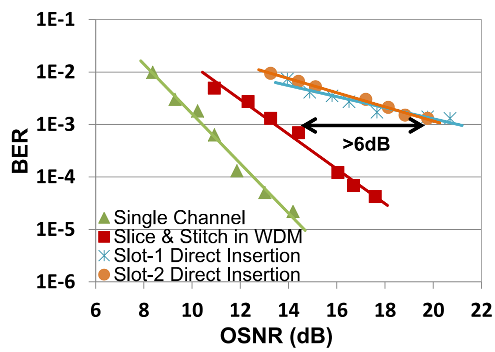

Fig. 13. BER comparison between direct channel insertion and fragmented bandwidth allocation enabled by channel slicing and stitching.

For further system evaluation, BER measurements of the added channel S are presented in Fig. 13. Compared to direct channel insertion, fragmented bandwidth allocation has more than 6 dB OSNR improvement at a BER of 1e-3. There is an additional OSNR penalty of channel slicing and stitching compared to the single-channel scenario. Similarly, a possible reason for this penalty could be that the filter for selecting a desired channel slice is not sharp enough to reject the adjacent channels.

VII. Conclusion and Discussion

This paper experimentally demonstrates a reconfigurable channel slicing and stitching for an optical signal to enable fragmented bandwidth allocation without O-E-O conversion. In a 6-channel WDM system, a 20 Gbaud optical channel is successfully reallocated into two fragmented frequency slots and reconstructed at the receiver. Although this scheme is demonstrated for an optical channel that is not pulse shaped, we believe the scheme might also be applicable to channels that are pulse shaped, e.g., Nyquist shaping.

In our experiment, there are different issues that could degrade the system performance, including: (i) the power of the optical signal is attenuated by the loss of different equipment, such as the PPLN (∼5 dB insertion loss) and the SLM filter (∼6 dB insertion loss); (ii) nonlinear wave mixing in both stages of the channel slicing and stitching requires sufficient signal power as provided by a 2W EDFA with a ∼6 dB noise figure; and (iii) there are optical components with limited bandwidth. We note that there are other approaches that could reduce channel bandwidth to fit into the smaller frequency slot, such as narrow filtering [16] or higher-order QAM signal conversion [17]. They may not suffer the same degradations as we have, but could introduce other issues.

The reason for using an optical frequency comb instead of independent continuous wave lasers is to ensure phase locking among different channel slices, which is generally required for successful signal recovery at the receiver. In our experiment, the selected comb lines (within a ∼10-nm spectrum range) have a similar OSNR of ∼30 dB. As the scheme is scaled to more channel slices with larger frequency spacing, the quality of the stitched signal might be affected by different OSNRs of different comb lines. In addition, we use the same comb source for both channel slicing and stitching for ease of experimentation; a more realistic implementation would likely use two independent comb sources for the transmitter and the receiver.

References

[1] M. Jinno *et al.*, “Distance-adaptive spectrum resource allocation in spectrum-sliced elastic optical path network [Topics in optical communications],” *IEEE Commun. Mag.*, vol. 48, no. 8, pp. 138–145, Aug. 2010.

[2] O. Gerstel, M. Jinno, A. Lord, and S. J. B. Yoo, “Elastic optical networking: a new dawn for the optical layer?,” *IEEE Commun. Mag.*, vol. 50, no. 2, pp. 12–20, Feb. 2012.

[3] K. Christodoulopoulos, I. Tomkos, and E. A. Varvarigos, “Elastic bandwidth allocation in flexible OFDM-Based optical networks,” *J. Lightw. Technol.*, vol. 29, no. 9, pp. 1354–1366, May 2011.

[4] B. Guo *et al.*, “Multicasting based optical inverse multiplexing in elastic optical network,” *Opt. Express*, vol. 22, no. 12, pp. 15133–15142, Jun. 2014.

[5] N. Sambo, F. Paolucci, G. Meloni, F. Fresi, L. Potì, and P. Castoldi, “Control of frequency conversion and defragmentation for super-channels [Invited],” *J. Opt. Commun. Netw.*, vol. 7, no. 1, pp. A126–A134, Jan. 2015.

[6] J. K. Fischer *et al.*, “Bandwidth-variable transceivers based on four-dimensional modulation formats,” *J. Lightw. Technol.*, vol. 32, no. 16, pp. 2886–2895, Aug. 2014.

[7] M. Jinno, H. Takara, B. Kozicki, Y. Tsukishima, Y. Sone, and S. Matsuoka, “Spectrum-efficient and scalable elastic optical path network: Architecture, benefits, and enabling technologies,” *IEEE Commun. Mag.*, vol. 47, no. 11, pp. 66–73, Nov. 2009.

[8] Y. Cao *et al.*, “Experimental demonstration of tunable optical channel slicing and stitching to enable dynamic bandwidth allocation,” in *Proc. Int. Conf. Exhib. Opt. Fiber Commun.*, Los Angeles, CA, USA, 2017, Paper Th1F.1.

[9] G. Lu, T. Bo, T. Sakamoto, N. Yamamoto, and C. Chan, “Flexible and scalable wavelength multicast of coherent optical OFDM with tolerance against pump phase-noise using reconfigurable coherent multi-carrier pumping,” *Opt. Express*, vol. 24, no. 20, pp. 22573–22580, Oct. 2016.

[10] Y. Cao *et al.*, “Pilot-tone-based self-homodyne detection using optical nonlinear wave mixing,” *Opt. Lett.*, vol. 42, no. 9, pp. 1840–1843, May 2017.

[11] S. J. Savory, “Digital filters for coherent optical receivers,” *Opt. Express*, vol. 16, no. 2, pp. 804–817, Jan. 2008.

[12] S. J. Savory, G. Gavioli, R. I. Killey, and P. Bayvel, “Electronic compensation of chromatic dispersion using a digital coherent receiver,” *Opt. Express*, vol. 15, no. 5, pp. 2120–2126, Mar. 2007.

[13] J. McNicol, M. O’Sullivan, K. Roberts, A. Comeau, D. McGhan, and L. Strawczynski, “Electrical domain compensation of optical dispersion [optical fibre communication applications],” in *Proc. Int. Conf. Opt. Fiber Commun.*, Anaheim, CA, USA, 2005, Paper OThJ3.

[14] B. J. C. Schmidt, A. J. Lowery, and J. Armstrong, “Experimental demonstrations of electronic dispersion compensation for long-haul transmission using direct-detection optical OFDM,” *J. Lightw. Technol.*, vol. 26, no. 1, pp. 196–203, Jan. 2008.

[15] G. Lu *et al.*, “Pump-phase-noise-free optical wavelength data exchange between QAM signals with 50-GHz channel-spacing using coherent DFB pump,” *Opt. Express*, vol. 24, no. 4, pp. 3702–3712, Feb. 2016.

[16] F. Fresi, M. Secondini, G. Berrettini, G. Meloni, and L. Potì, “Impact of optical and electrical narrowband spectral shaping in faster than Nyquist Tb superchannel,” *Photon. Technol. Lett.*, vol. 25, no. 23, pp. 2301–2303, Dec. 2013.

[17] G. Huang, Y. Miyoshi, A. Maruta, Y. Yoshida, and K. I. Kitayama, “All-optical OOK to 16-QAM modulation format conversion employing nonlinear optical loop mirror,” *J. Lightw. Technol.*, vol. 30, no. 9, pp. 1342–1350, May 2012.

Yinwen Cao received the B.S. and M.Eng. degrees from the Beijing University of Posts and Telecommunications, Beijing, China, in 2008 and 2011, respectively. He is currently working toward the Ph.D. degree in the Department of Electrical Engineering, University of Southern California, Los Angeles, CA, USA.

Ahmed Almaiman received the B.S. degree in electrical engineering from King Saud University, Riyadh, Saudi Arabia, in 2011, and the M.S. degree from the University of Southern California (USC), Los Angeles, CA, USA, in 2014. He is currently a Research Assistant in Optical Communications Laboratory, USC and is working toward the Ph.D. degree.

Morteza Ziyadi received the B.S. (Hons.) degree from Iran University of Science and Technology, Tehran, Iran, in 2008, and the M.S. (Hons.) degree from Sharif University of Technology, Tehran, in 2010, respectively, all in electrical engineering. He received the Doctorate degree in electrical engineering from the University of Southern California, Los Angeles, CA, USA, in 2017.

Amirhossein Mohajerin-Ariaei received the B.S. degree in electrical engineering from the Iran University of Science and Technology, Tehran, Iran, in 2009, and the M.S. degree in electrical engineering from the Sharif University of Technology, Tehran, in 2011. He is currently working toward the Ph.D. degree in electrical engineering at the University of Southern California, Los Angeles, CA, USA.

Changjing Bao has been working toward the Ph.D. degree in electrical engineering in the Department of Electrical Engineering, University of Southern California, Los Angeles, CA, USA, since 2012.

Peicheng Liao received the B.Eng. degree in optical engineering from Zhejiang University, Hangzhou, China, in 2012, and the M.Eng. degree in electrical and computer engineering from McGill University, Montreal, QC, Canada, in 2014. He is currently working toward the Ph.D. degree in electrical engineering in the University of Southern California, Los Angeles, CA, USA.

Fatemeh Alishahi received the B.S. degree in electrical engineering from the Shiraz University, Shiraz, Iran, in 2005, and the M.S. degree in electrical engineering from the Sharif University of Technology, Tehran, in 2008. She is currently working toward the Ph.D. degree in electrical engineering in the University of Southern California, Los Angeles, CA, USA.

Ahmad Fallahpour received the B.S. degree (Hons.) in electrical engineering from Shahid Beheshti University, Tehran, Iran, in 2012, and the M.S. degree in electrical engineering from the Sharif University of Technology, Tehran, in 2014. He is currently working toward the Ph.D. degree in electrical engineering in the University of Southern California, Los Angeles, CA, USA.

Youichi Akasaka received the B.S. degree in synthetic chemistry from Kyoto University, Kyoto, Japan, in 1988, and the M.S. and Ph.D. degrees in material science from the University of Tokyo, Tokyo, Japan, in 1990 and 1993, respectively. Since 2005, he has been a Senior Researcher working on advanced technologies for future photonic network at Fujitsu Laboratories of America, Richardson, TX, USA.

Dr. Akasaka is a senior member of the IEEE Photonics Society and received the Young Engineer Award from IEICE of Japan in 1995.

Carsten Langrock received the Ph.D. degree in electrical engineering from Stanford University, Stanford, CA, USA, in 2007. He has more than 150 publications, and is currently working as a Senior Research Scientist in Prof. Martin M. Fejer's Group in the Edward L. Ginzton Laboratory, Stanford University.

Martin M. Fejer received the B.A. degree in physics from Cornell University, Ithaca, NY, USA, and the Ph.D. degree in applied physics from Stanford University, Stanford, CA, USA. He is currently a Professor and the Department Chair of Applied Physics and served as a Senior Associate Dean for Natural Sciences at Stanford University. He has more than 500 publications and 30 patents.

Dr. Fejer is a Fellow of the Optical Society of America, and received the R.W. Wood prize in 1998. He was elected to the National Academy of Sciences in 2016.

Joseph D. Touch (SM'02) received the Ph.D. degree from the University of Pennsylvania, Philadelphia, PA, USA, and joined the Information Sciences Institute, University of Southern California (USC), Marina del Rey, CA, USA, in 1992. He is the Postel Center Director in USC's Information Sciences Institute and a Research Associate Professor in the USC's Computer Science and EE/Systems Departments.

Dr. Touch in Sigma Xi, an ACM Distinguished Scientist, and Senior Member of the Optical Society of America, and a ComSoc Distinguished Lecturer.

Moshe Tur (M'87–SM'94–F'98) received the B.Sc. degree in mathematics and physics from Hebrew University, Jerusalem, Israel, in 1969, the M.Sc. degree in applied physics from the Weizmann Institute of Science, Rehovot, Israel, in 1973, and the Ph.D. degree from Tel Aviv University, Tel Aviv, Israel, in 1981. He is currently the Gordon Professor of electrical engineering with the School of Electrical Engineering, Tel Aviv University, where he has established a fiber-Optic Sensing And Communication Laboratory. He has authored or coauthored more than 530 journal and conference technical papers.

Dr. Tur is a Fellow of the Optical Society of America.

Alan E. Willner (SM'94–F'04) received the Ph.D. degree from Columbia University, New York City, NY, USA, in 1988. He is currently the Steven and Kathryn Sample Chaired Professor in engineering with the University of Southern California, Los Angeles, CA, USA. He has more than 1100 publications and holds 30 patents.

Dr. Willner is a member of the U.S. National Academy of Engineering, an International Fellow of the U.K. Royal Academy of Engineering, and a Fellow of the National Academy of Inventors, the American Association for the Advancement of Science, the Optical Society, and SPIE.